Sub-anesthetic ketamine administration decreases deviance detection responses at the cellular, populational and mesoscale levels

Maria Isabel Carreño-Muñoz[1,2,*,#], Alessandra Ciancone Chama[1,2,*], Pegah Chehrazi[1,2], Bidisha Chattopadhyaya[2], Graziella Di Cristo[1,2,#]

Affiliations:

[1] Neurosciences Department, Université de Montréal ;

[2] Centre de Recherche, CHU Sainte-Justine (CHUSJ) ;

* Equal contribution

Corresponding authors:

Maria Isabel Carreño-Muñoz

Department of Neurosciences, Université de Montréal,

Centre de Recherche Azrieli, CHU Sainte-Justine,

3175, Côte-Sainte-Catherine, Montréal, QC H3T 1C5, Canada.

E-mail: maria.munoz.hsj@ssss.gouv.qc.ca

Graziella Di Cristo,

Department of Neurosciences, Université de Montréal,

Centre de Recherche, CHU Sainte-Justine,

3175, Côte-Sainte-Catherine, Montréal, QC H3T 1C5, Canada.

E-mail: graziella.dicristo.hsj@ssss.gouv.qc.ca

ABSTRACT

In the neocortex, neuronal processing of sensory events is significantly influenced by their predictability. A common example is the suppression of responses to repetitive stimuli in sensory cortices, a phenomenon known as habituation. Within a sensory information stream, whenever a novel stimulus deviates from expectations, enhanced brain responses are observed. Mismatch negativity (MMN), the electroencephalographic waveform reflecting rule violations, is a well-established biomarker for auditory deviant detection. MMN has been shown to depend on intact NMDA receptor signaling across species; nevertheless, the underlying mechanisms at the neuronal and mesoscale levels are still not fully understood. Using multi-electrode array recordings in awake mice, we identified a specific biphasic spiking response in a subpopulation of primary auditory cortex (A1) neurons elicited by deviant, but not standard, sounds, wherein the second peak is abolished by acute sub-anesthetic injection of ketamine, a partial non-competitive NMDA receptor antagonist. We further showed that the posterior parietal cortex (PPC), a critical hub for multisensory integration and sensorimotor coordination, responds to unexpected and deviant, but not repetitive, sounds, and this response is dependent upon intact NMDA receptor-mediated signaling. Finally, to explore the effects of ketamine on inter-cortical communication following deviance detection, we performed Granger Causality and Weighted Phase Lag Index analyses during the presentation of deviant and standard sounds. This analysis showed a unidirectional functional connectivity from A1 to PPC following deviant detection, which is impaired by ketamine administration. Altogether, our findings provide novel insights into the NMDA receptor-dependent mechanisms underlying the processing of novelty in auditory stimuli.

INTRODUCTION

Animal survival critically depends on the continuous updating of sensory information and its rapid processing to enable appropriate behaviors. To interact efficiently with ever-changing environments, mammalian brains must continuously align incoming sensory information with predictions based on current actions or intentions. Consequently, the brain has evolved various strategies to minimize computational demands while still efficiently navigating through a constant flow of information. One such strategy is the ability to suppress responses to predictable stimuli — a phenomenon referred to here as habituation, or stimulus-specific adaptation — while remaining alert to unexpected changes – referred to as deviance detection. In sensory cortices, neurons gradually reduce their firing to repetitive sounds but preserve robust responses to rare, deviant stimuli(Harms, Michie & Naatanen, 2016). This form of neuronal adaptation also manifests as changes in event-related potentials (ERPs), which are time-locked brain responses that represent changes at the population level in recorded local field potentials (LFP). As it is the case for neuronal firing, repetitive sounds also elicit a progressive reduction in ERP amplitude (Rosburg & Mager, 2021), while unexpected sounds trigger a specific wave shape response known as mismatch negativity (MMN)(Naatanen *et al.*, 2007), reflecting the brain's detection of deviations from auditory regularities. Together, auditory habituation and MMN both at the cellular and population level, provide a hierarchical framework for understanding how local neuronal response and large-scale network dynamics contribute to efficient sensory monitoring and predictive coding in the brain.

At the inter-cortical (mesoscale) level, recent studies have proposed that both functional and anatomical connectivity between distinct brain regions are essential for processing standard and deviant auditory stimuli. While several studies have emphasized the role of frontal cortex in top-down modulation of sound predictability (Hockley, Bohorquez & Malmierca, 2025), emerging evidence also highlights the potential involvement of the posterior parietal cortex (PPC), a higher-order associative region involved in both multisensory integration and sensorimotor coordination (Andersen & Buneo, 2002; Van Derveer, Ross & Hamm, 2023). Studies in rodents and humans have shown that the PPC exhibits robust responses to unexpected stimuli in the auditory domain (Justen & Herbert, 2018; Raltschev *et al.*, 2025).

Further, at the cellular level, PPC neurons can discriminate the presence or absence of expected auditory stimuli, in awake mice (Mohan *et al.*, 2018). However, it is still unknown how the PPC communicates with other cortical areas to contribute, at the mesoscale level, to the processing of rule violations.

Although the synaptic mechanisms underlying rule-violation processing are not completely understood yet, most studies propose N-methyl-D-aspartate (NMDA) receptor activity as a central mechanism (Light & Naatanen, 2013; Rosburg & Kreitschmann-Andermahr, 2016). For example, studies using sub-anesthetic doses of ketamine, a partial non-competitive antagonist of NMDA receptors, reliably reported reductions in MMN amplitude and auditory habituation in humans (Umbricht *et al.*, 2000; Kreitschmann-Andermahr *et al.*, 2001; Rosburg & Kreitschmann-Andermahr, 2016). While the effects of ketamine administration on MMN and auditory habituation at the local population level are relatively well documented, the impact of ketamine at the cellular and mesoscale levels, particularly in relation to functional inter-cortical connectivity and network dynamics, remains largely unexplored.

In this study, we assessed how a sub-anesthetic dose of ketamine affects auditory deviant detection and habituation at the population level, through ERP-MMN waveforms and evoked oscillatory activity analysis, and at the neural level, by analyzing single-unit firing, in the primary auditory cortex (A1) of awake mice. Furthermore, we explored the functional connectivity between PPC and A1 to gain a deeper understanding of the broader network dynamics involved both in auditory deviant detection and habituation.

MATERIAL AND METHODS

Animals

Experimental procedures involving mice were approved by the "Comité Institutionnel de Bonnes Pratiques Animales en Recherche" (CIBPAR) of the Research Center of Sainte-Justine Hospital in accordance with the principles published by the Canadian Council on Animal Care. Six adult C57Bl/6 mice (four males and two females) were used in this study. Mice were implanted at postnatal day (P)70–90 and recorded between P80 and P200. All

animals were housed with two to five mice/cage from weaning until surgery, after which they were singly housed for the duration of the experiment. Animals were kept on a 12h/12h light/dark cycle and provided with nesting material, food, and water *ad libitum*. All experiments were performed during the light period under constant mild luminosity (60 lx). We checked and noted the exact stage of the females' estrous cycle after each recording session by histological inspection of the vaginal smear (McLean *et al.*, 2012). To avoid variability and the concomitant effect of sex hormones, the two females included in our analysis were in the diestrus phase in all conditions (control, vehicle and ketamine).

Surgery

Cranial surgery was performed under deep anesthesia, induced by an intraperitoneal injection of ketamine/xylazine cocktail. Body temperature was maintained at 37°C using a feedback-controlled heating pad. Analgesics were given locally subcutaneously (Lidocaine 2%, Aspen Pharmacare, Canada) and an intraperitoneally dose of 30 mg/Kg (Buprenorphine, 0,3mg/ml, Vetergesic Multidose, Ceva) 5 min before surgery. Mice were head-fixed in a stereotaxic frame (Kopf Instruments, USA). During the entire surgery, eyes were protected and hydrated using Opticare eye lube (CLC Medica, Canada). The skull was exposed, cleaned, and treated with an activator (Metabond Quick, Parkell, USA). The coordinates of the targeted areas (described below) were marked with a permanent marker before fixing the skin around the exposed skull with Vetbond tissue adhesive (3M, USA). Then a first layer of dental cement (Metabond Quick, Parkell, USA) was applied to cover the whole exposed skull except the marked coordinates. Craniotomies were then performed above the targeted areas.

In the first set of experiments, custom-made clusters of four to six 50 µm-diameter-insulated-tungsten wires were implanted in every targeted area. In each one of those clusters, wire tips were 50–150 µm apart. A custom-designed and 3D-printed microdrive-like scaffold held the three electrode clusters at fixed positions previously described in(Carreno-Munoz *et al.*, 2022), thus allowing the simultaneous implantation of all three and reducing surgery time. In a second set of experiments, four independently movable tetrodes targeted the primary auditory cortex. Each tetrode was fabricated out of four 10 µm-diameter tungsten wires (H-Formvar insulation with Butyral bond coat California Fine Wire Company, Grover Beach, CA) that were twisted and then heated to bind them into a single bundle. The tips of the

tetrodes were then gold-plated to reduce the impedance to 200-400 kΩ. The use of tetrodes provides not only local field potential (LFP) recordings but also high-density spiking activity, allowing for the characterization of single-unit discharges. The 3D printed microdrives used were manufactured by Axona (Axona Ltd.; http://www.axona.com/).

A ground-and-reference wire was also gently introduced in the contralateral frontal lobe. The microdrive apparatus and the ground-and-reference wire were then daubed with dental acrylic (Ortho-Jet Powder and Jet liquid, Lang Dental, USA) to encase the electrode-microdrive assembly and anchor it to the skull. When implanting tetrodes, a drop of silicone elastomer (WPI, USA) was applied around the tetrodes before the acrylic to let tetrodes free for movement. For 1 week after surgery, animals were treated with Metacam and the skin around the implant was disinfected daily.

Coordinates

Electrode clusters were implanted at the following coordinates: primary auditory cortex (A1), −2.5 mm posterior to bregma, 3.9 mm lateral to the midline and 0.8 mm deep; primary visual cortex (V1), −4 mm posterior to bregma, 2 mm lateral to the midline, depth: 0.6 mm; posterior parietal cortex (PPC), −2 mm posterior to bregma,1.7 mm lateral to the midline, depth: 0.6 mm. Clusters placed in the V1 and PPC targeted both the supra and infragranular layers; those placed in the A1 targeted layer 5. Data shown in this study are specifically signal from layer 5 A1 and PPC.

EEG data acquisition

EEG recordings were performed using an open-ephys GUI platform (https://open-ephys.org/). Data was acquired at 20 KHz with a custom-made headstage using Intan Technologies RHD Electrophysiology Amplifier chip (https://intantech.com/products_RHD2000.html). Custom designed auditory and visual trigger generator devices sent triggers directly to the recording system, assuring the precise timing of stimuli presentation. Starting 1 week after surgery, animals were habituated daily for 4 days to an open field (15–20 min each time), before starting recordings for auditory stimulation protocols from Day 5. We used a dimly illuminated open field environment (45 × 35 cm), surrounded by 60 cm-high transparent walls, equipped with video monitoring. The

walls were sprayed and wiped clean with Peroxigard (Virox Technologies) 15 min before the introduction of each animal. Two speakers were placed ∼10 cm from the walls of the open field. Baseline activity was recorded at the beginning of each session for a period of 10 min, while mice were freely exploring the open field. EEG recordings during auditory stimulations were conducted for 20–30 min, a total of six to ten times, on alternate days.

Auditory stimulation protocols

All stimuli were presented at an intensity of 70-75 dB. The oddball paradigm comprised a sequence of five to nine repetitive (standard) sounds at 5 kHz, followed by a deviant sound at 10 kHz. Sequences were presented in a pre-established pseudo-random order. Sounds lasted 50ms and were presented with a 1s interstimulus interval. The full protocol lasted 10 min. Pure tone stimulation paradigm, consisted of a series of 500ms long, 5 and 10 kHz pure tones, presented with random interstimulus intervals of 2 to 5s. Each pure tone was presented 60 times in a random order. The full protocol lasted 5 min.

EEG preprocessing

EEG signals were down-sampled to 2000 Hz and a bandpass filter (0.5–150 Hz) was applied. A notch filter (59.5–60.5 Hz) was also applied to remove residual 60 Hz noise contamination. Data was then segmented into periods of different lengths, depending on the stimulation protocol: 1400ms (500ms pre- and 900ms post-stimulus onset) for the auditory oddball protocol, and 2500ms (1000ms pre- and 1500ms post-stimulus onset) for the pure tone stimulation. Trials with an intra-channel average higher than four times the total trial standard deviation (SD) were tagged, visually inspected and removed. Only sessions containing more than 50 clean trials were kept for further analyses.

Data analysis

None of the recorded animals were excluded from the final analysis. Signal analysis and quantification was performed using custom MATLAB (The Mathworks Inc.) codes, available upon request.

Evoked Related Potentials. The EEG signal was baseline corrected to the mean voltage at 100ms prior to stimulus onset and averaged over trials. The ERP components, baseline-to-peak N1, and absolute P1, were analyzed from the recorded evoked related potentials (ERPs).

The N1 amplitude was automatically detected by subtracting the minimum voltage (negative peak) within a 10-80ms time window after stimulus onset to the averaged baseline value. The P1 amplitude was calculated by measuring the maximum voltage (positive peak) within an 80-150ms time window after stimulus onset to the average baseline value. Analyses were carried out using the Fieldtrip toolbox (Oostenveld *et al.*, 2011). To quantify habituation from ERPs, we calculated the ratio between the N1 amplitudes of the first (S1) and the second (S2) standard sounds by dividing S2 by S1. These ratios were then converted to a logarithmic base 10 scale and multiplied by 10, using the following formula:

$$10 * log10(\frac{S2}{S1})$$

Mismatch negativity (MMN) trace was calculated by subtracting the EEG trace of the standard sound (S1) from the EEG trace of the deviant sound (D). The pattern obtained was then used to detect N1 (MMN-N1) and P1 (MMN-P1) amplitudes from each subject ERPs.

Power spectral density. Baseline power spectral density (PSD) analysis, was done during periods of immobility within the first 10 minutes of the recording session in the absence of any auditory stimuli. Immobility periods were defined by establishing a velocity threshold of the animal body center at <1 cm/s for at least 2 seconds. To estimate the power spectrum using Fast Fourier Transform (FFT), we used the Welsh method implemented in MATLAB. The estimated power spectrum was normalized by the total power of the signal and plotted using logarithmic scale for visualization purposes.

Evoked PSD analysis was performed on the 300ms following stimulation and baseline corrected using a similar formula than before:

$$10 * log10(\frac{FFT\ Baseline}{FFT\ Stimulation})$$

To adopt an approach comparable to the MMN trace and facilitate the comparison of habituation and deviant detection between experimental groups, we calculated the difference (Δ) in evoked PSD by subtracting the corresponding sound conditions: D − S1 (deviant detection) and S2 − S1 (habituation).

Spiking activity analysis. Offline processing of electrophysiological data began with the extraction of spikes from the high-pass filtered signal (800–5000 Hz) of recordings sampled at 20 kHz. Action potentials exceeding 5 standard deviations above the mean baseline were detected. Spike waveforms were then characterized by feature extraction, and putative neuronal units were identified using principal component analysis followed by automatic clustering using klustakwik(Harris *et al.*, 2000) (http://klustakwik.sourceforge.net/). Identified clusters were manually refined with a graphical cluster-cutting program(Csicsvari *et al.*, 1998). Only units exhibiting a clear refractory period (<2ms) in their auto-correlograms and well-isolated cluster boundaries were included in subsequent analyses.

Peri-stimulus time histograms (PSTH) and spike density function (SDF) were performed using the mlib toolbox by Maik Stüttgen (https://de.mathworks.com/matlabcentral/fileexchange/37339-mlib-toolbox-for-analyzing-spike-data). PSTH were calculated using a bin size of 5 ms. SDF were calculated by applying a gaussian distribution over the PSTH using a kernel of 1 ms width. Each neuron SDF was baseline corrected by subtracting SDF values during 50ms before the stimulus presentation from the entire SDF. Using this analysis, we identified 3 types of neurons, based on their firing behavior following the stimulus presentation: neurons that respond by increasing their firing (responding-excited), neurons that respond by decreasing their firing (responding-inhibited) and neurons whose firing does not change (non-responding neurons).

To facilitate the comparison of habituation and deviant detection between experimental groups, we calculated the difference (Δ) SDF by subtracting individual neurons SDF following deviant sound from SDF following standard sounds.

Connectivity analysis. Granger causality and Weighted Phase Lag Index (WPLI) analysis between A1 and PPC was also performed using the fieldtrip toolbox (Oostenveld *et al.*, 2011). Both analyses were performed during the MMN response period (80-320ms after the stimulus presentation) to avoid the first abrupt N1 peak and therefore the non-stationarity of the EEG signal. Both Granger causality and WPLI were calculated using a Fourier-based non-parametric spectral factorization approach, employing a multi-taper frequency transformation with DPSS tapers of order 5 and a padding factor of 3. As before, we

calculated the difference (Δ) in Granger causality and WPLI spectrograms by subtracting the spectrogram calculated during the periods following deviant sound (D) stimulation from those following standard sound (S1) stimulations.

RESULTS

Sub-anesthetic ketamine administration significantly reduces MMN response and auditory habituation.

To validate previous findings reporting a reduction of MMN responses in humans(Rosburg & Kreitschmann-Andermahr, 2016), primates (Gil-da-Costa *et al.*, 2013) and rodents(Schuelert *et al.*, 2018), we first assessed the effect of an acute sub-anesthetic dose of ketamine (8 mg/Kg) or vehicle on auditory MMN response and habituation in freely moving mice. The dose of ketamine selected was based on previous preclinical studies showing its rapid effects on cortical activity (Picard *et al.*, 2019). Six animals implanted with intracranial electrodes and familiarized with an open field arena were recorded before and after ketamine, or vehicle injection, during an auditory oddball paradigm consisting of a series of repetitive (standard) sounds randomly interrupted by deviant sounds (Figure 1A). We calculated MMN by subtracting the LFP trace of the standard sound from the LFP trace of the deviant sound. The positive deflection in this waveform, peaking at approximately 100-250ms after stimulus onset, is known as the MMN response, and it has been proposed to reflect the brain's automatic detection of rule-violations of auditory regularities. Our results show that ketamine, but not vehicle, administration significantly reduced the amplitude of MMN response, corresponding to the P1 component of the MMN waveform (Figure 1C, D). This data is consistent with previously reported observations in humans (Rosburg & Kreitschmann-Andermahr, 2016), primates(Gil-da-Costa *et al.*, 2013) and rodents (Schuelert *et al.*, 2018), thus validating our model. Acute ketamine administration did not induce a reduction of MMN N1 amplitude (first negative peak), as a previous study reported (Ehrlichman *et al.*, 2008), although acute vehicle injection did significantly reduce MMN N1 amplitude (Figure 1C, D).

Acute ketamine injection, but not vehicle, also significantly disrupted auditory habituation to standard sounds (Figure 1F), measured as the ratio between the N1 amplitude of the first (S1) and the second (S2) standard sounds, validating previous observations in humans (de la Salle *et al.*, 2022). Since higher doses of ketamine administration can induce hyperlocomotion (de la Salle *et al.*, 2022) and previous studies showed that auditory processing is modulated by motor activity (Schneider, Nelson & Mooney, 2014; Bigelow *et al.*, 2019), we measured the total distance traveled by each mouse during the whole recording session. We found no effect of ketamine or vehicle injection on mouse locomotion (Figure 1G), thus ruling out an effect of altered motor activity on auditory processing.

Sub-anesthetic ketamine administration significantly reduces the late component of spiking activity response.

To further understand the effect of ketamine on MMN responses at the cellular level, we analyzed concomitant neuronal activity during oddball protocol stimulation after vehicle or ketamine injection. To do so, we identified spiking activity of individual neurons and evaluated their firing rates by calculating their peri-stimulus time histograms (PSTH, Figure 2A, lower panels) and spike density functions (Figure 2B). Our results show three different populations, based on their firing behavior following the deviant sound onset: neurons that respond by increasing their firing (responding-excited, Figure 2A-D), neurons that respond by decreasing their firing (responding-inhibited, Figure 2E-H) and neurons whose firing does not change (non-responding neurons, therefore not analyzed further). In naïve mice, deviant, but not standard sounds induced a biphasic response in the spiking activity of A1 neurons that were excited by the sounds (Figure 2B). This response was characterized by a fast and early burst of activity peaking at 25ms after stimulus onset, followed by a slow and late response at 100-200ms after stimulus onset, sharing common temporal dynamics with the MMN response. This observation is in line with previous reports (Chen, Helmchen & Lutcke, 2015), suggesting that the second late component of spiking activity may code for novelty in A1 neurons (Ulanovsky, Las & Nelken, 2003) as well as those in other regions such as in the substantia nigra (Mikell *et al.*, 2014) and PFC (Camalier *et al.*, 2019). To facilitate comparison between experimental groups, we calculated the difference (Δ) in spike density

functions (SDF) by subtracting the standard sound condition (S1) from the deviant sound condition (D). We refer to this subtractive measure as Δ SDF (Figure 2C, 2G). Analysis of Δ SDF showed that ketamine, but not vehicle, administration completely abolished this novelty-related late component of the spiking activity response (Figure 2D), therefore specifically affecting the saliency of the novel stimuli but not its deviant nature within the sequence of sounds.

Conversely, neurons that were inhibited specifically by deviant sounds showed a slower and monophasic negative response that was not affected by ketamine administration (Figure 2E-H). These findings indicate that there are at least two different neuronal populations in A1 which differ in their sensitivity to ketamine. Moreover, they reveal that stimulus-specific inhibitory responses may persist despite reduced NMDA signaling, while novelty-specific excitatory responses require intact NMDA receptor function, suggesting a critical role for NMDA-mediated synaptic transmission in encoding auditory novelty.

Oscillatory activity evoked by deviant sounds is significantly reduced by sub-anesthetic ketamine administration.

Recordings from primary sensory areas across species shows that sensory stimulation reliably evokes a response in the gamma spectrum (centered at 40Hz), reflecting enhanced sensory processing during early perceptual encoding (Mulert *et al.*, 2007; Naatanen *et al.*, 2007; Polomac *et al.*, 2015; Picard *et al.*, 2019). To investigate whether ketamine administration affects this response in A1, we evaluated the oscillatory activity following standard and deviant sound presentations. Although the baseline oscillatory activity was similar between groups (Figure 3A-B), naive animals showed a strong response at 40Hz evoked specifically by deviant, but not standard, sounds (Figure 3C, left). To facilitate comparing the response in the different experimental groups, we calculated the difference (Δ) in evoked PSD, (referred to as Δ PSD), by subtracting the following sound conditions: deviant minus S1 (deviant detection) and S2 minus S1 (habituation) (Figure 3D, 3E). Ketamine, but not vehicle, administration was sufficient to significantly reduce the evoked 40Hz response in the Δ PSD (Figure 3D, 3E). Of note, following ketamine administration, the response at 40Hz evoked by standard sounds appears higher than in naïve or vehicle-

injected mice (Figure 3C), consistent with previous reports showing that ketamine increases the evoked responses to standard sounds (Kreitschmann-Andermahr *et al.*, 2001; Lee *et al.*, 2018). We further evaluated habituation by comparing evoked oscillatory activity during S1 and S2. Contrary to what was observed in naïve or vehicle-injected mice (Figure 3F, left), evoked responses at 40Hz during S2 were significantly reduced following ketamine administration (Figure 3G-H). Consistent with our data, previous studies have shown that ketamine impairs evoked gamma (~40 Hz) responses to sounds presented at random inter-trial intervals (Schuelert *et al.*, 2018; Curic *et al.*, 2019). Therefore, altogether, these results suggest that sub-anesthetic ketamine generally disrupts the brain's ability to respond to unpredictable stimuli in auditory input streams.

Posterior parietal cortex response to deviant sounds requires NMDA receptor-mediated signaling.

Emerging evidence suggests that the PPC, a higher-order associative region involved in both multisensory integration and sensorimotor coordination (Andersen & Buneo, 2002; Van Derveer, Ross & Hamm, 2023), is implicated in top-down modulation of sound predictability (Hockley, Bohorquez & Malmierca, 2025). Therefore, we next investigated whether PPC integrates rule violation in the auditory stream. We observed that PPC robustly responds to deviant sounds, while its response to standard sounds is negligible (Figure 4A, D). To rule out the possibility that the differential response to the standard vs deviant sound is not due to the intrinsic nature of the sounds (5 kHz vs. 10 kHz) but only attributable to their predictability, we presented these two sounds with a randomized order and inter-trial interval. Notably, when the two sounds were unpredictable, PPC robustly responded to both 5kHz and 10kHz sounds (Supplementary figure 1), indicating that the PPC specifically responds to unexpected and deviant auditory stimuli, but not to standard sounds. Next, we analyzed MMN waves (D-S1) and observed a prominent P1 peak in naïve mice, similar to A1. Ketamine (Figure 4A-C), but not vehicle (Figure 4D-F), administration induced a significant reduction of the MMN P1 response in the PPC, again concurrent to findings in A1. Similarly, MMN N1 amplitude was not significantly affected by ketamine nor vehicle injection (Figure 4C, F). Furthermore, neither ketamine nor vehicle administration had any significant

influence on auditory habituation (Figure 4G-J), suggesting that the PPC is not involved in habituation responses to repetitive stimuli. These results indicate that PPC integrates rule-violation stimuli and its responses to deviant sounds require intact NMDA receptor-mediated signaling.

Sub-anesthetic ketamine administration disrupts A1 to PPC functional connectivity elicited by auditory deviance detection.

To explore the effects of ketamine on inter-cortical communication during deviance detection, we performed Granger causality and weighted Phase Lag Index (wPLI) analyses during the presentation of deviant and standard sounds. Granger causality analysis quantifies the directional influence between time series by determining whether past values of one signal improve the prediction of future values of another (Bastos & Schoffelen, 2015). WPLI, on the other hand, assesses the phase synchronization between signals, offering a robust measure of functional connectivity (Vinck *et al.*, 2011). We applied both methods to the time window corresponding to the MMN response (80-320ms after stimuli presentation), a time window chosen to avoid erratic or sudden changes in the signal due to the non-stationary nature of the evoked potentials.

To compare the responses in the different experimental groups, we calculated the subtraction index (Δ) for deviance detection (D-S1) and habituation (S2-S1) using both analysis methods (referred to as Δ Granger and Δ wPLI in Figure 5, Supplementary figure 3). The analysis of Δ Granger (Figure 5) showed an increased connectivity between A1 and PPC at 40 Hz, which was evident specifically during deviant but not standard sounds (Supplementary figure 2). These results suggest an important role of A1-PPC connectivity underlying deviance detection but not habituation. Of note, this communication at 40 Hz was disrupted following ketamine, but not vehicle, administration (Figure 5A, Supplementary figure 2). Granger causality analysis further highlighted the directional nature of this communication which appeared to be exclusively from A1 to PPC, with no reciprocal influence in the opposite direction. These results on A1-PPC functional connectivity were also replicated and confirmed via WPLI analysis (Supplementary figure 3).

Overall, this data suggests that rule violation in the auditory stream elicits functional communication from A1 to PPC, which is dependent on intact NMDA-mediated signaling.

DISCUSSION

The core concept of predictive coding theory suggests that the brain generates a model of the environment based on its previous experiences and forms a predictive coding framework. Incoming sensory information is continuously referenced to this internal predictive model, and cases of mismatch give rise to a prediction error signal. The auditory oddball paradigm (repeating standard sounds randomly interrupted by rare deviant stimuli) has been routinely used to elucidate how the brain encodes regular auditory patterns, generates inherent models of predictability and uses it to efficiently detect deviations from these internal models (Naatanen *et al.*, 2007; Fitzgerald & Todd, 2020).

MMN, the electrophysiological response to rule violations, is a well-established biomarker of auditory deviant detection, whereby an auditory evoked potential to a deviant stimulus is greater than the response to repetitive standard stimuli. Using this approach, we found that sub-anesthetic ketamine administration significantly reduced the amplitude of the auditory MMN response, specifically the P1 component, without affecting N1. In addition, oscillatory analyses further revealed that ketamine markedly reduced the 40 Hz response selectively evoked by deviant sounds, impairing both novelty detection and habituation at the gamma-band level. These findings validate previous work demonstrating that MMN depends on intact NMDA receptor signaling across species (Umbricht *et al.*, 2000; Gil-da-Costa *et al.*, 2013; Chen, Helmchen & Lutcke, 2015; Javitt & Sweet, 2015; Rosburg & Kreitschmann-Andermahr, 2016; Schuelert *et al.*, 2018). Nevertheless, the underlying neural and inter-cortical network mechanisms are still under debate. To bridge this gap, our study extends beyond classical population-level measures by uncovering the cellular correlates of deviance detection and the mesoscale connectivity that links primary sensory and associative cortices.

Our results at the cellular level show that the firing response of a subpopulation of A1 neurons follows a biphasic pattern: a rapid initial peak shortly after stimulus presentation, followed by a slower later peak (between 100ms and 250ms), that coincides with the timing of the MMN response at the population level. This biphasic pattern consistently appeared during

deviant sounds, while standard sounds only elicited fast monophasic responses. Furthermore, sub-anesthetic ketamine administration significantly and specifically reduced the second peak of spiking activity following the presentation of a deviant sound. These data suggest that ketamine administration has a selective effect on the second later peak of the response, presumably reflecting a higher-order realization of sound processing. We speculate that the slower, ketamine-sensitive peak of neuronal firing could be due to disinhibition of cortical excitatory activity due to a greater NMDA sensitivity of inhibitory circuits (Grunze *et al.*, 1996; Li *et al.*, 2002; Homayoun & Moghaddam, 2007; Middleton *et al.*, 2008; Widman & McMahon, 2018; Picard *et al.*, 2019). For example, previous studies have shown that sub-anesthetic ketamine administration preferentially inhibits PV+ interneurons, by targeting NMDA receptors containing the 2A subunit, and regulates evoked gamma-band oscillations in visual cortex (Picard *et al.*, 2019). This inhibitory effect of ketamine on PV+ interneurons could indeed explain our observations of a reduced evoked 40Hz response to deviant sounds, since reduced evoked 40Hz rhythms have been linked to PV+ interneuron hypofunction (Cardin *et al.*, 2009; Picard *et al.*, 2019; Batista-Brito *et al.*, 2023). Additionally, long-range callosal PV+ neurons have been shown to play a critical role in inter-area connectivity, in different cortical regions, including the prefrontal (Cho *et al.*, 2023) and auditory cortex (Zurita, Feyen & Apicella, 2018). Other GABAergic interneurons populations, including VIP and SST+ interneurons have been also involved in disinhibitory mechanisms mediated by neuromodulators (reviewed in Kullander & Topolnik, 2021); however, whether and how the activity of different interneuron populations is affected by acute sub-anesthetic ketamine treatment remains to be elucidated. Interestingly, sub-anesthetic ketamine administration can bidirectionally modulate cortical acetylcholine levels (Kikuchi *et al.*, 1997; Kim *et al.*, 1999). Cholinergic, and in particular, nicotinic stimulation has been demonstrated to enhance MMN amplitudes (Harkrider & Hedrick, 2005; Inami *et al.*, 2005; Inami *et al.*, 2007; Martin, Davalos & Kisley, 2009; Hamilton *et al.*, 2018; Weber *et al.*, 2022). Therefore, altered basal forebrain to A1 communication, possibly through cross-talk with dis-inhibitory microcircuits could contribute to the specific effect of ketamine on the slower later peak of spiking activity.

The second peak of A1 neuron firing elicited by the deviant sound could be also mediated by astrocytic signaling. For example, in the lateral habenula, foot-shock stress has been shown to induce a bimodal neuronal response, similarly to what we observed in A1 neurons

following deviant sounds (Xin *et al.*, 2025). In this region, the second peak of neuronal activation was shown to be mediated by astrocytic release of the gliotransmitters glutamate and ATP/adenosine (Xin *et al.*, 2025). Further, a recent study has shown that neuromodulators can signal through astrocytes to modulate synapse strength in adult mouse hippocampus (Lefton *et al.*, 2025). Whether astrocytic signaling contribute to MMN responses in A1 is thus far unknown.

Recent studies emphasize the importance of whole-brain connectivity for processing auditory stimuli. While the frontal cortex has been extensively studied for its role in top-down control of prediction errors (Hockley, Bohorquez & Malmierca, 2025), far less is known about the PPC. As a hub for multisensory integration (Choi & Lee, 2025) and higher-order auditory processing (Andersen & Buneo, 2002; Van Derveer, Ross & Hamm, 2023), the PPC has been shown to respond to unexpected sounds (Justen & Herbert, 2018; Mohan *et al.*, 2018; Raltschev *et al.*, 2025); however, its precise role in differentiating redundant from deviant auditory stimuli remains largely unexplored. In this study, we show that while PPC exhibited a strong response to both unexpected and deviant sounds, its response to repetitive sounds was negligible. Notably, ketamine administration did not affect the N1 component, yet abolished the P1 component of the MMN, which is thought to carry the novelty content of the response. Based on this observation, we focused our connectivity analyses on the late response period. By using both Granger causality and wPLI analysis, we provide, to the best of our knowledge, the first evidence that functional connectivity from A1 to PPC supports auditory deviance detection, highlighting a previously uncharacterized mesoscale pathway for rule-deviation processing. We further show that this process is dependent on intact NMDA signaling. This effect may arise because ketamine administration abolishes the functional connectivity from A1 to PPC, by altering either A1 local circuits primarily and/or A1 to PPC projections. Overall, our observations are consistent with previous studies reporting decreased directed functional connectivity across the brain under various psychedelics drugs (Muthukumaraswamy *et al.*, 2015; Barnett *et al.*, 2020). These data further support the hypothesis that the psychedelic state involves a breakdown in patterns of functional organization or information flow in the brain (Barnett *et al.*, 2020).

Paradoxically, ketamine's ability to restore impaired cortical networks, particularly in regions such as the prefrontal cortex, is considered central to its antidepressant effects in treatment-resistant depression (Li *et al.*, 2016; Roussy *et al.*, 2021); Abdallah *et al.*, 2017; Gass *et al.*, 2019). This may be due to the specific nature of the underlying pathophysiology of treatment-resistant depression. Intriguingly, MMN has been shown to be impaired in psychiatric disorders such as depression (Tseng, Nouchi & Cheng, 2021) and schizophrenia (Molnar *et al.*, 2024), both of which have been linked to NMDA receptor dysfunction, although in opposite directions. In schizophrenia, NMDA receptor hypofunction is thought to contribute to reduced MMN amplitude and sensory processing deficits, while in depression, NMDA receptor hyperfunction is believed to underlie similar sensory processing disruptions (Balu, 2016; Adell, 2020; Wang *et al.*, 2022). Although, the therapeutic mechanisms behind ketamine's anti-depressive effects are still not well understood, they are thought to involve multiple parallel mechanisms, including altered neurotransmission through NMDA receptor antagonism, enhanced synaptic plasticity and modulation of various signaling pathways, such as the mTOR pathway (Duman *et al.*, 2016).

In summary, our data identify a specific biphasic spiking response in a subpopulation of A1 neurons elicited by deviant, but not standard sounds, with the second peak dependent on NMDA receptor–mediated signaling. The identity of the neurons participating in this response and the underlying microcircuit mechanisms remain to be elucidated. We further provide evidence that the PPC responds to unexpected and deviant, but not repetitive, sounds and that this response is dependent on NMDA receptors. Finally, we demonstrate a uni-directional functional connectivity from A1 to PPC likely contributing to the integration of deviant sounds, which is abolished by sub-anesthetic ketamine administration. Together, these data support the hypothesis that PPC, through intact NMDA receptor signaling, contributes to the mesoscale network underlying prediction error processing. By bridging cellular, population, and mesoscale levels, our study offers the first integrated evidence of how NMDA-dependent auditory circuits shape rule-deviation processing, unveiling a previously uncharacterized pathway for novelty detection. Further studies are needed to understand the precise role of A1-PPC connectivity and PPC itself in the processing of rule-violation processing.

ACKNOWLEDGEMENTS

We would like to thank Kristian Agbogba, Mikael Valton Charette and James Waldron for their technical assistance, the Comité Institutionnel de Bonne Pratiques Animales en Recherche (CIBPAR), all the personnel of the animal facility of the Research Center of CHU Sainte-Justine (Université de Montreal) and Compute Canada for their instrumental technical support and members of our lab for insightful data discussion. We would also like to thank Dr Jozsef Csicsvari and his lab for sharing their spike sorting analysis pipeline. This work was supported by the Natural Sciences and Engineering Research Council of Canada (NSERC) and La Fondation des Étoiles (G.DC.); the Canadian Neurodevelopmental Research Training (CanNRT) Platform (M.I.C-M and A.C.C) and the Savoy Foundation fellowship (M.I.C-M).

DATA AVAILABILITY. All data and codes are available upon request.

CONFLICT OF INTERESTS. The authors declare no conflicts of interest.

AUTHORS CONTRIBUTION. MIC-M, ACC, GDC designed the experiments. MIC-M, ACC, PC performed the experiments. MIC-M, ACC analyzed data. MIC-M, ACC, BC, GDC wrote the manuscript. All authors read and corrected the manuscript.

REFERENCES

Abdallah, C.G., Averill, L.A., Collins, K.A., Geha, P., Schwartz, J., Averill, C., DeWilde, K.E., Wong, E., Anticevic, A., Tang, C.Y., Iosifescu, D.V., Charney, D.S. & Murrough, J.W. (2017) Ketamine Treatment and Global Brain Connectivity in Major Depression. *Neuropsychopharmacology*, **42**, 1210-1219.

Adell, A. (2020) Brain NMDA Receptors in Schizophrenia and Depression. *Biomolecules*, **10**.

Andersen, R.A. & Buneo, C.A. (2002) Intentional maps in posterior parietal cortex. *Annu Rev Neurosci*, **25**, 189-220.

Balu, D.T. (2016) The NMDA Receptor and Schizophrenia: From Pathophysiology to Treatment. *Adv Pharmacol*, **76**, 351-382.

Barnett, L., Muthukumaraswamy, S.D., Carhart-Harris, R.L. & Seth, A.K. (2020) Decreased directed functional connectivity in the psychedelic state. *Neuroimage*, **209**, 116462.

Bastos, A.M. & Schoffelen, J.M. (2015) A Tutorial Review of Functional Connectivity Analysis Methods and Their Interpretational Pitfalls. *Front Syst Neurosci*, **9**, 175.

Batista-Brito, R., Majumdar, A., Nuno, A., Ward, C., Barnes, C., Nikouei, K., Vinck, M. & Cardin, J.A. (2023) Developmental loss of ErbB4 in PV interneurons disrupts state-dependent cortical circuit dynamics. *Mol Psychiatry*.

Bigelow, J., Morrill, R.J., Dekloe, J. & Hasenstaub, A.R. (2019) Movement and VIP Interneuron Activation Differentially Modulate Encoding in Mouse Auditory Cortex. *eNeuro*, **6**.

Camalier, C.R., Scarim, K., Mishkin, M. & Averbeck, B.B. (2019) A Comparison of Auditory Oddball Responses in Dorsolateral Prefrontal Cortex, Basolateral Amygdala, and Auditory Cortex of Macaque. *J Cogn Neurosci*, **31**, 1054-1064.

Cardin, J.A., Carlen, M., Meletis, K., Knoblich, U., Zhang, F., Deisseroth, K., Tsai, L.H. & Moore, C.I. (2009) Driving fast-spiking cells induces gamma rhythm and controls sensory responses. *Nature*, **459**, 663-667.

Carreno-Munoz, M.I., Chattopadhyaya, B., Agbogba, K., Cote, V., Wang, S., Levesque, M., Avoli, M., Michaud, J.L., Lippe, S. & Di Cristo, G. (2022) Sensory processing dysregulations as reliable translational biomarkers in SYNGAP1 haploinsufficiency. *Brain*, **145**, 754-769.

Chen, I.W., Helmchen, F. & Lutcke, H. (2015) Specific Early and Late Oddball-Evoked Responses in Excitatory and Inhibitory Neurons of Mouse Auditory Cortex. *J Neurosci*, **35**, 12560-12573.

Cho, K.K.A., Shi, J., Phensy, A.J., Turner, M.L. & Sohal, V.S. (2023) Long-range inhibition synchronizes and updates prefrontal task activity. *Nature*, **617**, 548-554.

Choi, I. & Lee, S.H. (2025) Locomotion-dependent auditory gating to the parietal cortex guides multisensory decisions. *Nat Commun*, **16**, 2308.

Csicsvari, J., Hirase, H., Czurko, A. & Buzsaki, G. (1998) Reliability and state dependence of pyramidal cell-interneuron synapses in the hippocampus: an ensemble approach in the behaving rat. *Neuron*, **21**, 179-189.

Curic, S., Leicht, G., Thiebes, S., Andreou, C., Polomac, N., Eichler, I.C., Eichler, L., Zollner, C., Gallinat, J., Steinmann, S. & Mulert, C. (2019) Reduced auditory evoked gamma-band response and schizophrenia-like clinical symptoms under subanesthetic ketamine. *Neuropsychopharmacology*, **44**, 1239-1246.

de la Salle, S., Choueiry, J., McIntosh, J., Bowers, H., Ilivitsky, V. & Knott, V. (2022) N-methyl-D-aspartate receptor antagonism impairs sensory gating in the auditory cortex in response to speech stimuli. *Psychopharmacology (Berl)*, **239**, 2155-2169.

Duman, R.S., Aghajanian, G.K., Sanacora, G. & Krystal, J.H. (2016) Synaptic plasticity and depression: new insights from stress and rapid-acting antidepressants. *Nat Med*, **22**, 238-249.

Ehrlichman, R.S., Maxwell, C.R., Majumdar, S. & Siegel, S.J. (2008) Deviance-elicited changes in event-related potentials are attenuated by ketamine in mice. *J Cogn Neurosci*, **20**, 1403-1414.

Fitzgerald, K. & Todd, J. (2020) Making Sense of Mismatch Negativity. *Front Psychiatry*, **11**, 468.

Gass, N., Becker, R., Reinwald, J., Cosa-Linan, A., Sack, M., Weber-Fahr, W., Vollmayr, B. & Sartorius, A. (2019) Differences between ketamine's short-term and long-term effects on brain circuitry in depression. *Transl Psychiatry*, **9**, 172.

Gil-da-Costa, R., Stoner, G.R., Fung, R. & Albright, T.D. (2013) Nonhuman primate model of schizophrenia using a noninvasive EEG method. *Proc Natl Acad Sci U S A*, **110**, 15425-15430.

Grunze, H.C., Rainnie, D.G., Hasselmo, M.E., Barkai, E., Hearn, E.F., McCarley, R.W. & Greene, R.W. (1996) NMDA-dependent modulation of CA1 local circuit inhibition. *J Neurosci*, **16**, 2034-2043.

Hamilton, H.K., D'Souza, D.C., Ford, J.M., Roach, B.J., Kort, N.S., Ahn, K.H., Bhakta, S., Ranganathan, M. & Mathalon, D.H. (2018) Interactive effects of an N-methyl-d-aspartate receptor antagonist and a nicotinic acetylcholine receptor agonist on mismatch negativity: Implications for schizophrenia. *Schizophr Res*, **191**, 87-94.

Harkrider, A.W. & Hedrick, M.S. (2005) Acute effect of nicotine on auditory gating in smokers and non-smokers. *Hear Res*, **202**, 114-128.

Harms, L., Michie, P.T. & Naatanen, R. (2016) Criteria for determining whether mismatch responses exist in animal models: Focus on rodents. *Biol Psychol*, **116**, 28-35.

Harris, K.D., Henze, D.A., Csicsvari, J., Hirase, H. & Buzsaki, G. (2000) Accuracy of tetrode spike separation as determined by simultaneous intracellular and extracellular measurements. *J Neurophysiol*, **84**, 401-414.

Hockley, A., Bohorquez, L.H. & Malmierca, M.S. (2025) Top-down prediction signals from the medial prefrontal cortex govern auditory cortex prediction errors. *Cell Rep*, **44**, 115538.

Homayoun, H. & Moghaddam, B. (2007) NMDA receptor hypofunction produces opposite effects on prefrontal cortex interneurons and pyramidal neurons. *J Neurosci*, **27**, 11496-11500.

Inami, R., Kirino, E., Inoue, R. & Arai, H. (2005) Transdermal nicotine administration enhances automatic auditory processing reflected by mismatch negativity. *Pharmacol Biochem Behav*, **80**, 453-461.

Inami, R., Kirino, E., Inoue, R., Suzuki, T. & Arai, H. (2007) Nicotine effects on mismatch negativity in nonsmoking schizophrenic patients. *Neuropsychobiology*, **56**, 64-72.

Javitt, D.C. & Sweet, R.A. (2015) Auditory dysfunction in schizophrenia: integrating clinical and basic features. *Nat Rev Neurosci*, **16**, 535-550.

Justen, C. & Herbert, C. (2018) The spatio-temporal dynamics of deviance and target detection in the passive and active auditory oddball paradigm: a sLORETA study. *BMC Neurosci*, **19**, 25.

Kikuchi, T., Wang, Y., Shinbori, H., Sato, K. & Okumura, F. (1997) Effects of ketamine and pentobarbitone on acetylcholine release from the rat frontal cortex in vivo. *Br J Anaesth*, **79**, 128-130.

Kim, S.H., Price, M.T., Olney, J.W. & Farber, N.B. (1999) Excessive cerebrocortical release of acetylcholine induced by NMDA antagonists is reduced by GABAergic and alpha2-adrenergic agonists. *Mol Psychiatry*, **4**, 344-352.

Kreitschmann-Andermahr, I., Rosburg, T., Demme, U., Gaser, E., Nowak, H. & Sauer, H. (2001) Effect of ketamine on the neuromagnetic mismatch field in healthy humans. *Brain Res Cogn Brain Res*, **12**, 109-116.

Kullander, K. & Topolnik, L. (2021) Cortical disinhibitory circuits: cell types, connectivity and function. *Trends Neurosci*, **44**, 643-657.

Lee, M., Balla, A., Sershen, H., Sehatpour, P., Lakatos, P. & Javitt, D.C. (2018) Rodent Mismatch Negativity/theta Neuro-Oscillatory Response as a Translational Neurophysiological Biomarker for N-Methyl-D-Aspartate Receptor-Based New Treatment Development in Schizophrenia. *Neuropsychopharmacology*, **43**, 571-582.

Lefton, K.B., Wu, Y., Dai, Y., Okuda, T., Zhang, Y., Yen, A., Rurak, G.M., Walsh, S., Manno, R., Myagmar, B.E., Dougherty, J.D., Samineni, V.K., Simpson, P.C. & Papouin, T. (2025) Norepinephrine signals through astrocytes to modulate synapses. *Science*, **388**, 776-783.

Li, C.T., Chen, M.H., Lin, W.C., Hong, C.J., Yang, B.H., Liu, R.S., Tu, P.C. & Su, T.P. (2016) The effects of low-dose ketamine on the prefrontal cortex and amygdala in treatment-resistant depression: A randomized controlled study. *Hum Brain Mapp*, **37**, 1080-1090.

Li, Q., Clark, S., Lewis, D.V. & Wilson, W.A. (2002) NMDA receptor antagonists disinhibit rat posterior cingulate and retrosplenial cortices: a potential mechanism of neurotoxicity. *J Neurosci*, **22**, 3070-3080.

Light, G.A. & Naatanen, R. (2013) Mismatch negativity is a breakthrough biomarker for understanding and treating psychotic disorders. *Proc Natl Acad Sci U S A*, **110**, 15175-15176.

Martin, L.F., Davalos, D.B. & Kisley, M.A. (2009) Nicotine enhances automatic temporal processing as measured by the mismatch negativity waveform. *Nicotine Tob Res*, **11**, 698-706.

McLean, A.C., Valenzuela, N., Fai, S. & Bennett, S.A. (2012) Performing vaginal lavage, crystal violet staining, and vaginal cytological evaluation for mouse estrous cycle staging identification. *J Vis Exp*, e4389.

Middleton, S., Jalics, J., Kispersky, T., Lebeau, F.E., Roopun, A.K., Kopell, N.J., Whittington, M.A. & Cunningham, M.O. (2008) NMDA receptor-dependent

switching between different gamma rhythm-generating microcircuits in entorhinal cortex. *Proc Natl Acad Sci U S A*, **105**, 18572-18577.

Mikell, C.B., Sheehy, J.P., Youngerman, B.E., McGovern, R.A., Wojtasiewicz, T.J., Chan, A.K., Pullman, S.L., Yu, Q., Goodman, R.R., Schevon, C.A. & McKhann, G.M., 2nd (2014) Features and timing of the response of single neurons to novelty in the substantia nigra. *Brain Res*, **1542**, 79-84.

Mohan, H., Gallero-Salas, Y., Carta, S., Sacramento, J., Laurenczy, B., Sumanovski, L.T., de Kock, C.P.J., Helmchen, F. & Sachidhanandam, S. (2018) Sensory representation of an auditory cued tactile stimulus in the posterior parietal cortex of the mouse. *Sci Rep*, **8**, 7739.

Molnar, H., Marosi, C., Becske, M., Bekesi, E., Farkas, K., Stefanics, G., Czigler, I. & Csukly, G. (2024) A comparison of visual and acoustic mismatch negativity as potential biomarkers in schizophrenia. *Sci Rep*, **14**, 992.

Mulert, C., Leicht, G., Pogarell, O., Mergl, R., Karch, S., Juckel, G., Moller, H.J. & Hegerl, U. (2007) Auditory cortex and anterior cingulate cortex sources of the early evoked gamma-band response: relationship to task difficulty and mental effort. *Neuropsychologia*, **45**, 2294-2306.

Muthukumaraswamy, S.D., Shaw, A.D., Jackson, L.E., Hall, J., Moran, R. & Saxena, N. (2015) Evidence that Subanesthetic Doses of Ketamine Cause Sustained Disruptions of NMDA and AMPA-Mediated Frontoparietal Connectivity in Humans. *J Neurosci*, **35**, 11694-11706.

Naatanen, R., Paavilainen, P., Rinne, T. & Alho, K. (2007) The mismatch negativity (MMN) in basic research of central auditory processing: a review. *Clin Neurophysiol*, **118**, 2544-2590.

Oostenveld, R., Fries, P., Maris, E. & Schoffelen, J.M. (2011) FieldTrip: Open source software for advanced analysis of MEG, EEG, and invasive electrophysiological data. *Comput Intell Neurosci*, **2011**, 156869.

Picard, N., Takesian, A.E., Fagiolini, M. & Hensch, T.K. (2019) NMDA 2A receptors in parvalbumin cells mediate sex-specific rapid ketamine response on cortical activity. *Mol Psychiatry*, **24**, 828-838.

Polomac, N., Leicht, G., Nolte, G., Andreou, C., Schneider, T.R., Steinmann, S., Engel, A.K. & Mulert, C. (2015) Generators and Connectivity of the Early Auditory Evoked Gamma Band Response. *Brain Topogr*, **28**, 865-878.

Raltschev, C., Kasavica, S., Leonardon, B., Nevian, T. & Sachidhanandam, S. (2025) Top-down modulation of sensory processing and mismatch in the mouse posterior parietal cortex. *Nat Commun*, **16**, 4240.

Rosburg, T. & Kreitschmann-Andermahr, I. (2016) The effects of ketamine on the mismatch negativity (MMN) in humans - A meta-analysis. *Clin Neurophysiol*, **127**, 1387-1394.

Rosburg, T. & Mager, R. (2021) The reduced auditory evoked potential component N1 after repeated stimulation: Refractoriness hypothesis vs. habituation account. *Hear Res*, **400**, 108140.

Roussy, M., Luna, R., Duong, L., Corrigan, B., Gulli, R.A., Nogueira, R., Moreno-Bote, R., Sachs, A.J., Palaniyappan, L. & Martinez-Trujillo, J.C. (2021) Ketamine disrupts naturalistic coding of working memory in primate lateral prefrontal cortex networks. *Mol Psychiatry*, **26**, 6688-6703.

Schneider, D.M., Nelson, A. & Mooney, R. (2014) A synaptic and circuit basis for corollary discharge in the auditory cortex. *Nature*, **513**, 189-194.

Schuelert, N., Dorner-Ciossek, C., Brendel, M. & Rosenbrock, H. (2018) A comprehensive analysis of auditory event-related potentials and network oscillations in an NMDA receptor antagonist mouse model using a novel wireless recording technology. *Physiol Rep*, **6**, e13782.

Tseng, Y.J., Nouchi, R. & Cheng, C.H. (2021) Mismatch negativity in patients with major depressive disorder: A meta-analysis. *Clin Neurophysiol*, **132**, 2654-2665.

Ulanovsky, N., Las, L. & Nelken, I. (2003) Processing of low-probability sounds by cortical neurons. *Nat Neurosci*, **6**, 391-398.

Umbricht, D., Schmid, L., Koller, R., Vollenweider, F.X., Hell, D. & Javitt, D.C. (2000) Ketamine-induced deficits in auditory and visual context-dependent processing in healthy volunteers: implications for models of cognitive deficits in schizophrenia. *Arch Gen Psychiatry*, **57**, 1139-1147.

Van Derveer, A.B., Ross, J.M. & Hamm, J.P. (2023) Robust multisensory deviance detection in the mouse parietal associative area. *Curr Biol*, **33**, 3969-3976 e3964.

Vinck, M., Oostenveld, R., van Wingerden, M., Battaglia, F. & Pennartz, C.M. (2011) An improved index of phase-synchronization for electrophysiological data in the presence of volume-conduction, noise and sample-size bias. *Neuroimage*, **55**, 1548-1565.

Wang, S., Bian, L., Yin, Y. & Guo, J. (2022) Targeting NMDA Receptors in Emotional Disorders: Their Role in Neuroprotection. *Brain Sci*, **12**.

Weber, L.A., Tomiello, S., Schobi, D., Wellstein, K.V., Mueller, D., Iglesias, S. & Stephan, K.E. (2022) Auditory mismatch responses are differentially sensitive to changes in muscarinic acetylcholine versus dopamine receptor function. *Elife*, **11**.

Widman, A.J. & McMahon, L.L. (2018) Disinhibition of CA1 pyramidal cells by low-dose ketamine and other antagonists with rapid antidepressant efficacy. *Proc Natl Acad Sci U S A*, **115**, E3007-E3016.

Xin, Q., Wang, J., Zheng, J., Tan, Y., Jia, X., Ni, Z., Xu, Z., Feng, J., Wu, Z., Li, Y., Li, X.M., Ma, H. & Hu, H. (2025) Neuron-astrocyte coupling in lateral habenula mediates depressive-like behaviors. *Cell*, **188**, 3291-3309 e3224.

Zurita, H., Feyen, P.L.C. & Apicella, A.J. (2018) Layer 5 Callosal Parvalbumin-Expressing Neurons: A Distinct Functional Group of GABAergic Neurons. *Front Cell Neurosci*, **12**, 53.

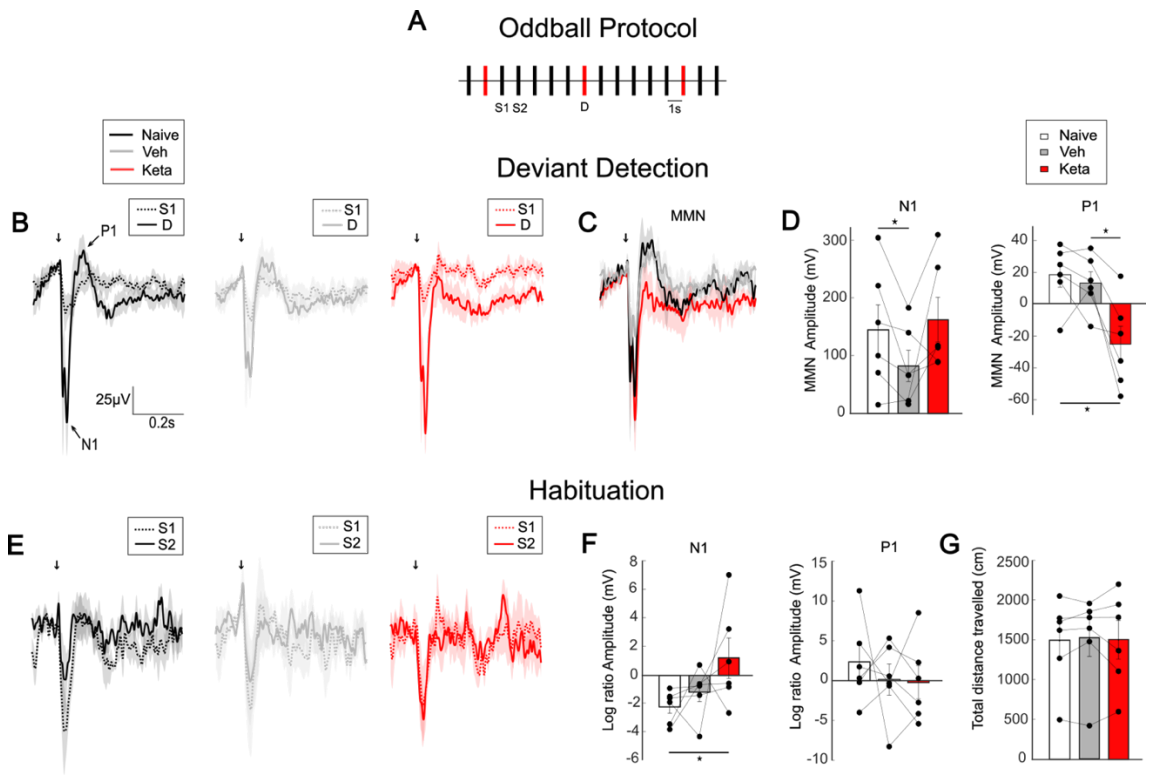

Figure 1. Sub-anesthetic ketamine alters MMN responses during deviant detection and stimulus specific adaption. (**A**) Schematic representation of the oddball protocol with black bars representing 5kHz pure tones (standard sounds) and the red bars 10kHz pure tones (deviant sounds). (**B**) Mean AEP (auditory evoked potentials) traces of standard (dotted) and deviant (solid) sounds for naive (left), vehicle injected (middle), and low-dose ketamine injected (right) mice. Arrows indicate the start time of stimulation. N1 is identified as the first negative peak ~10-20 ms and P1 as the first positive peak ~30-40 ms. (**C**) Superposed MMN (deviant—standard) traces. (**D**) Bar plots of MMN N1 (Naive-Keta Wilcoxon signed ranked test; z=0.314, p=0.753; Naive-Veh Wilcoxon signed ranked test; z =-1.992, p=0.046; Veh-Keta Wilcoxon signed ranked test; z =1.572, p =0.116) and MMN P1 (Ctrl-Keta Wilcoxon signed ranked test: z=-2.201, p=0.028; Naive-Veh Wilcoxon signed ranked test; z =-0.943, p =0.345; Veh-Keta Wilcoxon signed ranked test: z=2.201, p=0.028) peak amplitude. (**E**) Mean response to the first (dotted) and second (solid) standard sound for naive (left), vehicle injected (middle), and low-dose ketamine injected (right) mice. (**F**) Bar plots show N1(Naive-Keta Wilcoxon signed ranked test; z =2.201, p=0.028; Naive-Veh Wilcoxon signed ranked test; z =1.363, p=0.173; Veh-Keta Wilcoxon signed ranked test; z =1.363, p=0.173) and P1(Ctrl-Keta Wilcoxon signed ranked test; z =-0.524, p=0.600; Naive-Veh Wilcoxon signed ranked test; z =-0.105, p=0.917; Veh-Keta Wilcoxon signed ranked test; z=-0.314, p=0.753) amplitude after first (S1) versus second (S2) sounds in mice. (**G**) Bar plot of total distance travelled (Ctrl-Keta Wilcoxon signed ranked test; z=0.105, p=0.917; Naive-Veh Wilcoxon signed ranked test; z =0.734, p=0.463; Veh-Keta Wilcoxon signed ranked test; z =-0.105, p=0.917). Naïve mice, n = 6; Vehicle-injected mice, n = 6; Ketamine-injected mice, n = 6.

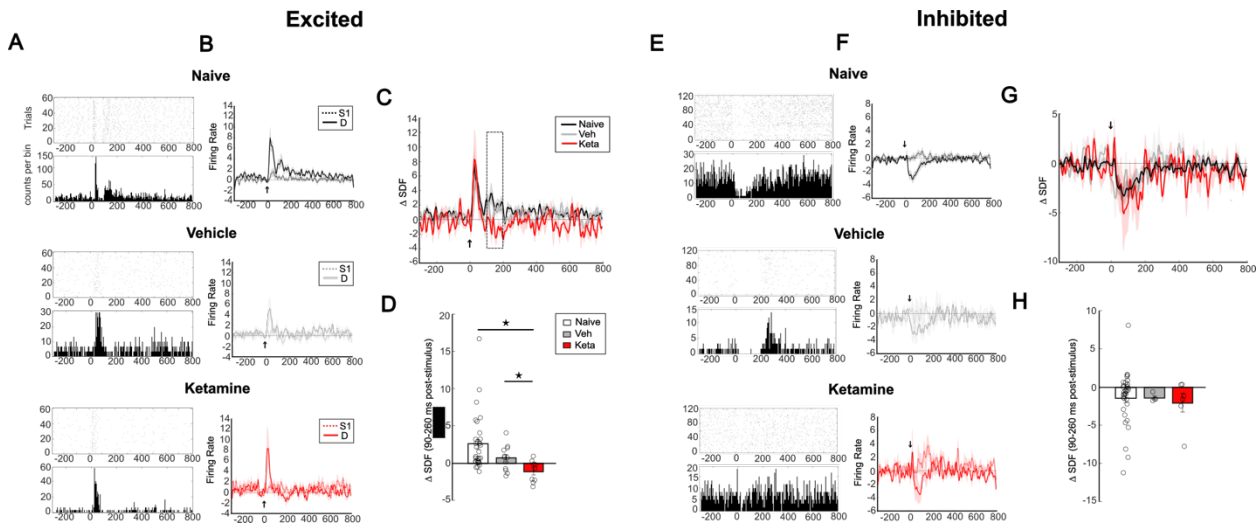

Figure 2. Sub-anesthetic ketamine alters spiking activity of responding neurons during deviant detection and stimulus specific adaptation. (**A**, **E**) Raster plots (top) and PTSH (bottom) for representative responding excited (**A**) and inhibited (**E**) neurons in naïve (top-black), vehicle injected (middle-gray), and ketamine injected (bottom-red) mice. (**B**, **F**) Firing probability of responding excited (**B**) and inhibited (**F**) neurons in each condition. (**C**, **G**) Spike density function of the MMN of responding excited (**C**) and responding inhibited (**G**) neurons in naive (top), vehicle injected (middle), and ketamine injected (bottom) mice. (**D**, **H**) Bar plots of MMN evoked firing responses of responding excited cells (**D**; Naive-Keta Linear mixed model: p=0.034, mean difference=2.950, std. error=1.346; Naive-Veh Linear mixed model: p= 0.029, mean difference= 1.549, std.error=0.658; Veh-Keta Linear mixed model: p=0.323, mean difference=-1.18, std.error=1.18)) and responding inhibited cells (**H**; Naive-Keta Linear mixed model: p= 0.660, mean difference= 0.584, std. error=1.317; Naive-Veh Linear mixed model: p=0.791, mean difference=0.383, std.error=1.432; Veh-Keta Linear mixed model: p=0.639, mean difference=0.674, std.error=1.384)). Responding excited neurons: n=36 cells from 5 mice (naïve), n=12 cells from 4 mice (vehicle-injected), and n= 9 cells from 5 mice (ketamine-injected). Responding inhibited neurons: n=33 cells from 5 mice (naive), n=4 cells from 2 mice (vehicle-injected), and n= 6 cells from 4 mice (ketamine-injected.

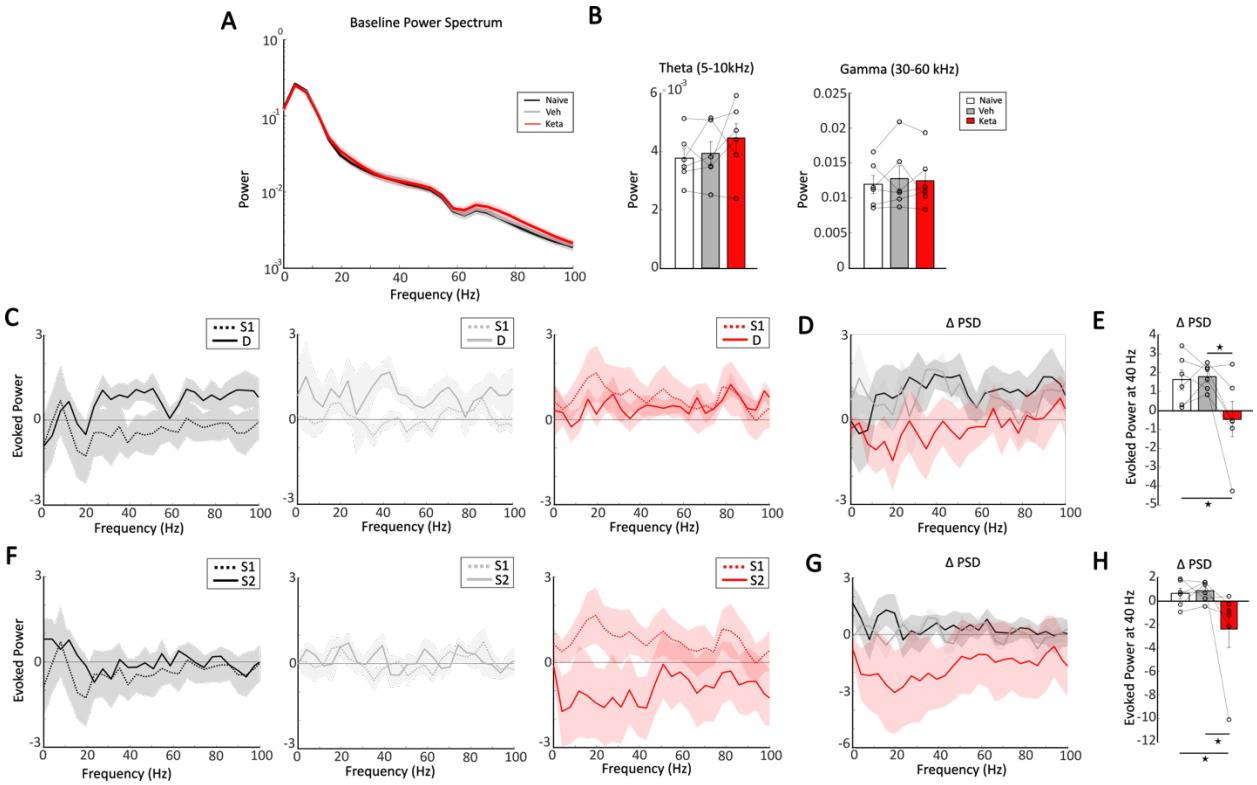

Figure 3. Sub-anesthetic ketamine affects power density spectra during deviance detection. (**A**) Power density spectra (5–100Hz) of 3-min baseline state (non-stimulus) EEG signal from the auditory cortex. (**B**) Bar plots show mean powers ± SEM of the theta (Naive- Keta Wilcoxon signed ranked test: z= 0.524, p=0.600; Veh-Keta Wilcoxon signed ranked test: z=-0.105, p=0.917; Ctrl-Veh Wilcoxon signed ranked test: z=0.943, p=0.345) and gamma (Naive- Keta Wilcoxon signed ranked test: z=1.572, p=0.116; Veh-Keta Wilcoxon signed ranked test: z=0.943, p=0.345; Ctrl-Veh Wilcoxon signed ranked test: z=0.524, p=0.600) bands in mice. (**C**) Evoked power in response to standard and deviant sounds in naive (left), vehicle-injected (middle), and ketamine-injected (right) mice. (**D**) MMN of evoked power in response to standard and deviant sounds across all frequencies. (**E**) Bar plot of MMN of evoked power at 40 Hz (Naive- Keta Wilcoxon signed ranked test: z= -2.201, p=0.028; Veh-Keta Wilcoxon signed ranked test: z=1.992, p=0.046; Naive-Veh Wilcoxon signed ranked test: z=-0.524, p=0.600). (**F**) Evoked power in response to the first (S1) and second (S2) standard sounds in naive (left), vehicle-injected (middle), and ketamine-injected (right) mice. (**G**) Evoked power of the log ratio of the second and first standard sounds across all frequencies (S2/S1). (**H**) Bar plot of S2/S1 log ratio evoked power at 40 Hz (Naive-Keta Wilcoxon signed ranked test: z= -2.201, p=0.028; Veh-Keta Wilcoxon signed ranked test: z=1.992, p=0.046; Naïve-Veh Wilcoxon signed ranked test: z=0.524, p=0.600). Naïve mice, n = 6; Vehicle-injectes mice, n = 6; Ketamine-injected mice, n = 6.

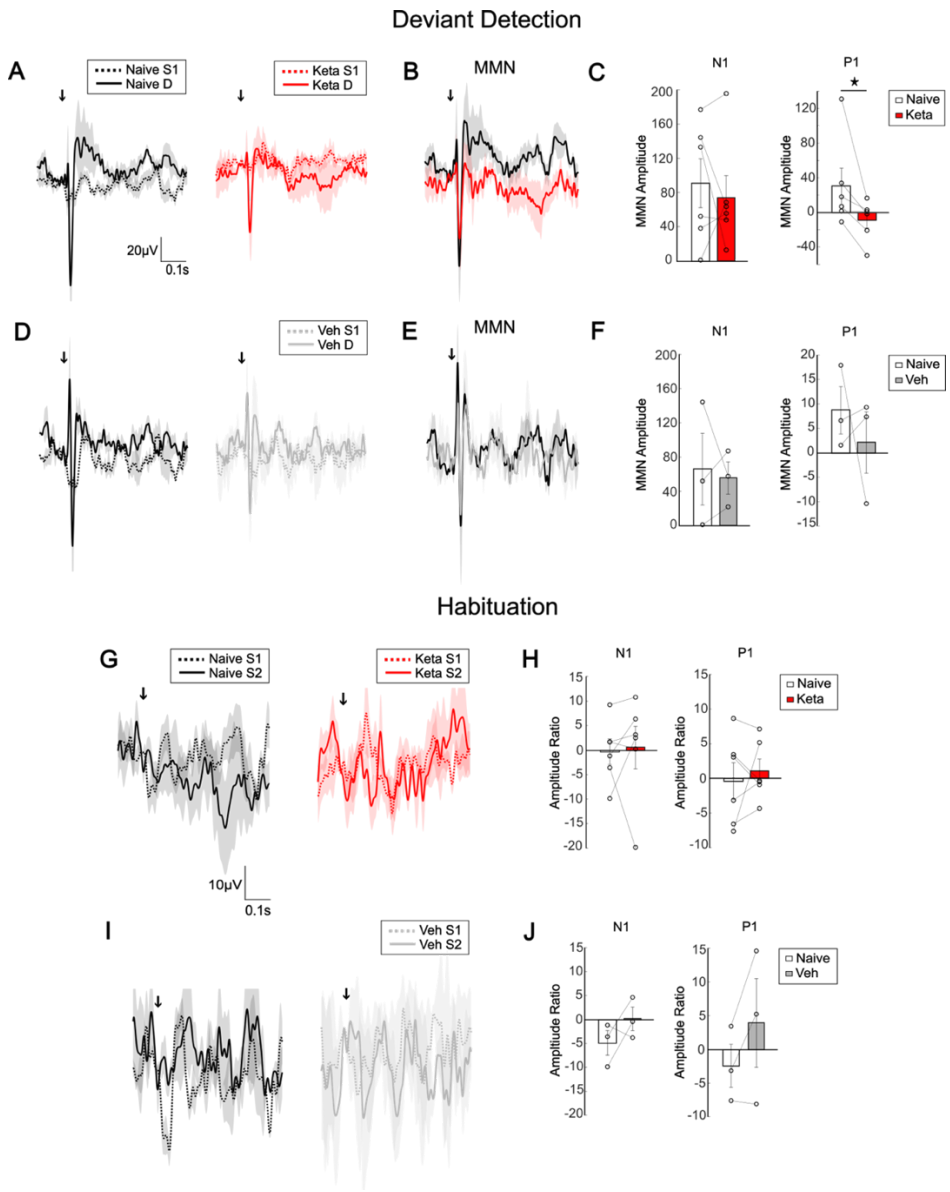

Figure 4. PPC encodes deviance detection. (**A**, **B**) Deviant detection in the PPC of naive vs ketamine injected mice. (**A**) Mean AEP traces of standard (dotted) and deviant (solid) sounds for naive (left) versus low-dose ketamine injected (right) mice. (**B**) Superposed MMN (deviant-standard) traces. (**C**) Bar plots of MMN N1 (Wilcoxon signed ranked test: z=-0.314, p=0.753) and MMN P1 (Wilcoxon signed ranked test: z=-2.201, p=0.028) peak amplitude in naive and ketamine-injected mice. (**D-F**) Deviant detection in the PPC of naive vs vehicle-injected mice. (**D**) Mean AEP traces of standard (dotted) and deviant (solid) sounds for naive (left) and vehicle injected (right) mice. (**E**) Superposed MMN (deviant—standard) traces. (**F**) Bar plots of MMN N1 (Wilcoxon signed ranked test: z=-2.201, p=0.028) and MMN P1(Wilcoxon signed ranked test: z=0.0, p=1.00). (**G**) Mean AEP traces of the first (dotted) and second (solid) standard sounds for naïve (left) versus ketamine-injected (right) mice. (**H**) Bar plots of S2/S1 log ratio N1(Wilcoxon signed ranked test: z=0.524, p=0.600) and P1 (Wilcoxon signed ranked test: z=105, p=0.917) peak amplitude in naive and ketamine-injected mice. (**I**) Mean AEP traces of the first (dotted) and

second (solid) standard sounds for naive (left) versus vehicle injected (right) mice. (J) Bar plots of S2/S1 log ratio N1(Wilcoxon signed ranked test: z=1.069, p=0.285) and P1 (Wilcoxon signed ranked test: z=1.069, p=0.285) peak amplitude in naive and ketamine-injected mice. Naive (n=6) versus Ketamine-injected (n=6) mice; naive(n=3) versus Vehicle-injected (n=3) mice.

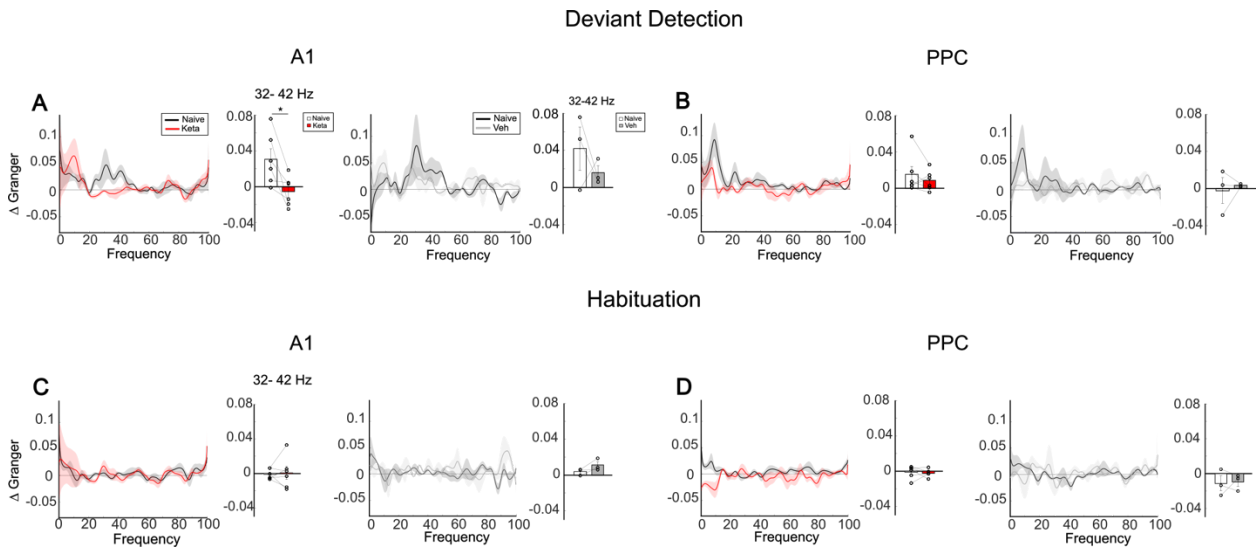

Figure 5. Sub-anesthetic ketamine decreases predictive connectivity from A1 to PPC. (A, B) Granger causality during deviant detection. Granger causality of MMN (deviant-standard) (left) and bar plot of their Granger index at 32-42 Hz (right) from A1 to PPC (**A**) and from PPC to A1 (**B**) for naive versus ketamine-injected mice (left) (Wilcoxon signed ranked test: z= -2.201, p=0.028) and naive versus vehicle-injected mice (right) (Wilcoxon signed ranked test: z= -1.069, p=0.285) mice. (**C**, **D**) Granger causality during auditory habituation. Granger causality of the log ratio of the second and first standard sounds (S2/S1) and bar plot of their Granger index at 32-42 Hz from A1 to PPC (**C**) and from PPC to A1 (**D**) for naive versus ketamine-injected mice (left) (Wilcoxon signed ranked test: z= -0.734, p=0.463) and Naive versus vehicle-injected mice (right) (Wilcoxon signed ranked test: z= 0.00, p=1.00) mice. Naive (n=6) versus Ketamine-injected (n=6) mice; naive (n=3) versus Vehicle-injected (n=3) mice.